JOURNAL OF SPACECRAFT AND ROCKETS
Vol. 39, No. 5, September–October 2002

Dimensional Repeatability of an Elastically Folded Composite Hinge for Deployed Spacecraft Optics

Jeanette L. Domber,* Jason D. Hinkle,† and Lee D. Peterson‡
University of Colorado, Boulder, Colorado 80309-0429
and
Peter A. Warren§
Foster-Miller, Inc., Waltham, Massachusetts 02154-1196

A new type of folded composite hinge is investigated for its use in precision deployable spacecraft structures. The hinge is an integral feature of a composite tube intended for use as a structural truss member. The design of the hinge allows the tube to be elastically folded for stowage even with tube wall thicknesses from 0.4 to 1.7 mm. Whether the large but primarily elastic folding stresses impart permanent deformations to the tube after it is deployed is experimentally assessed. The data show that any such permanent strain induces tip deformations, identified as microscopic plastic behavior, of no more than 2.5 μ axially and 9 μ laterally, depending on the composite layup. This deployment repeatability is comparable to prior measurements of mechanical deployables. Moreover, stow duration and number of stows have no measurable effect, once the initial stow–deploy cycle has been completed. There is always a significant viscoelastic creep recovery following deployment that increases with stowage time. However, this viscoelastic creep is recovered. An exponential curve fit of the creep time response shows that the time constants of the viscoelastic recovery are independent of stow duration.

Nomenclature

$\{a\}$	=	vector of coefficients, μm
b	=	intercept, μm
k	=	spring stiffness constant, N/m
M	=	model order
m	=	thermal correlation coefficient, μm/°C
N	=	number of measurements
P	=	probability
S_x	=	sample standard deviation, μm
t	=	time, s
$t_{\nu,P}$	=	Student's t distribution
u_x	=	precision interval, μm
y	=	tip displacement, μm
$\hat{y}$	=	tip displacement estimate, μm
ΔT	=	change in temperature, °C
ν	=	degrees of freedom
σ_i^2	=	sample variance, μm^2
τ	=	time constant, s
$\{\tau\}$	=	vector of time constants, s
χ^2	=	chi-squared distribution

Presented as Paper 2001-1539 at the AIAA/ASME/ASCE/AHS 43rd Structures, Structural Dynamics, and Materials Conference, Seattle, WA, 16–19 April 2001; received 5 July 2001; revision received 22 January 2002; accepted for publication 18 April 2002.

*Graduate Research Assistant, Center For Aerospace Structures 429 UCB, Department of Aerospace Engineering Sciences; Jeanette.Domber@colorado.edu. Student Member AIAA.

†Research Associate, Center For Aerospace Structures 429 UCB, Department of Aerospace Engineering Sciences; Jason.Hinkle@colorado.edu. Member AIAA.

‡Associate Professor, Center For Aerospace Structures 429 UCB, Department of Aerospace Engineering Sciences; Lee.Peterson@colorado.edu. Associate Fellow AIAA.

§Senior Engineer, Structures and Transportation Group, 350 Second Avenue; pwarren@foster-miller. com. Member AIAA.

Introduction

FUTURE large-aperture space telescopes will require deployable structures with high stiffness, high stability, and compact stowage.[1] Such spacecraft may need to deploy a 10-m-class mirror with overall stability at the nanometer scale. A common architecture being considered for such structures uses mechanical hinge and latch components to permit folding and packaging of the structure. Research has shown that mechanical joints can achieve the often conflicting design requirements of stiffness, nanometer-scale stability, and micrometer-scale repeatability.[2]

Nevertheless, this performance is imperfect and usually comes with added mass and complexity in the mechanisms.[3] As the size of the structures scale upward, the relative mass due to mechanisms might become a significant fraction of the total mass of the structure. Also, a precision mechanism is often a complicated mechanism, with carefully designed load paths, flexures, and actuators. For these reasons, alternatives to mechanical hinges might, in some cases, offer design advantages, if they can be adapted to the high stiffness and precision required by these applications.

Elastically folded structures, such as the hinge studied in this paper, offer one such possible alternative. Elastically folded structures are widely used in spacecraft structures today, although not at the nanometer scale of precision required for space observatories. For example, the BI-STEM, commonly used for deployable spacecraft booms, is a single piece of material folded by opening its slit circular cross-section until it becomes flat and then rolling the material onto a spool.[4–6] Another example of an elastically folded mechanism is a tape hinge, which is routinely used today in spacecraft.[7,8] The mechanics, stability, stiffness, and design of these concepts have been widely studied in the literature under macroscopic (submillimeter to meter) scales of deformation.

The integral folding hinge studied in this paper represents a new type of elastically folded structure. The hinge is actually an integral feature of a graphite composite tube intended for use as a truss member. The design of the hinge allows the tube to be elastically folded for stowage even for tube wall thicknesses between 0.4 and 1.7 mm and diameters between 70.3 and 88.6 mm. Integral hinge truss elements such as these can be assembled either alone or in combination with mechanical hinges to form complete deployable truss structures. Most important, they allow deeper, higher stiffness metering structures to be folded into reduced volumes, something that can be difficult for high-precision mechanical hinges. Unlike BI-STEMS and tape springs, this hinge can have high stiffness and

still be elastically folded. This attribute makes the integral folding hinge appropriate for consideration in high-precision deployable structures.

One of the immediate concerns about using an integral folding hinge in a precision structure is whether the significant, though elastic, stresses induced during folding result in a microscopic permanent deformation of the hinge. Even though bulk failure of the hinge does not occur, the stresses in the folded state may induce nonrecoverable deformation due to creep and anelastic instability in the composite material. If this anelastic behavior is manifested as a permanent deformation that exceeds the stroke capability of active optical elements, the hinge may be unsuitable for precision applications.

There appears to be little relevant prior work on the topic of microscopic yielding in composite structural components. Although the failure mechanisms of composite materials have been studied extensively, to the knowledge of the authors, the literature has been limited to delamination and impact mechanics. The concern addressed here is microscopic scales of yielding under an otherwise macroscopically elastic stress field. Although the literature lacks references in this regard concerning composites, there is extensive precedence for such concern in metallic alloys. For example, the "microyield" stress in a metal is often used to limit the loading of optical components to very low stresses, on the order of tens or hundreds of pounds per square inch, so that permanent, microscopic yield in the material is avoided.[9]

This paper contributes the first study of the microscopic yielding of composites, as manifested in a folded, high stiffness composite hinge. This yielding is measured as the magnitude of the dimensional repeatability of the hinge after being folded and unfolded, or stowed and then deployed. Three different composite layups are compared. Postdeployment position is measured with nanometer-level accuracy.

Following deployment, all specimens exhibited a viscoelastic recovery that increased with longer durations of stowage. However, once this viscous recovery was completed, very little residual deformation remained in the specimens. This residual deformation defines the deployment repeatability, or the microscopic yielding, of the specimen. For different composite layups, the deployment repeatability varied between 0 and 2.5 μm axially and between 0.1 and 9 μm laterally. In addition, there did not appear to be a sensitivity to stow duration or number of stows. This level of deployment repeatability is comparable to prior measurements of mechanical deployables.

The paper is organized as follows: The next section of the paper describes the integral folding hinge. This description is limited somewhat by the proprietary nature of the design, but sufficient information is provided to compare the repeatability with other designs. The experiments conducted to assess the deployment repeatability of the test articles are then described, and results from the experiments are presented. Finally, a model is extracted from the viscous decay to show that the recovery is apparently linear viscoelasticity with invariant time constants, to the level of resolution of these experiments.

Integral Folding Hinge

The integral folding hinge is a composite structure formed through a combination of geometry and tailored fiber orientation that limits the material stresses in the folded state. The hinge deploys under the strain energy that remains in the stowed condition. Both deployed and stowed configurations are diagrammed in Fig. 1. In the folded state, the hinge is folded to a net stow angle of approximately 160 deg. The composite consists of a polyetheretherketone (PEEK^{TM}) matrix reinforced with either IM7 or AS4 carbon fibers aligned in various proprietary configurations. Typical properties for these materials are listed in Table 1 (see Ref. 10).

Although the specific configuration of the hinge and the manufacturing processes are proprietary, these details are unimportant to the present investigation. What is important is that the configuration achieves a very low stress in the folded state. Based on the properties of the cross section and the material, the maximum principal stress in the fibers that is induced by folding is estimated to be 569 MPa. This induced stress is less than 18% of the elastic yield limit of the composite, which was calculated using standard composite theory to combine the yield strength of IM7 carbon fibers and PEEK resin to be 3100 MPa.

Table 2 provides the geometry and layups of the test specimens. Specimen 1 was measured in a conventional material test apparatus to have an extensional stiffness of 5.8 MN/m. The theoretical stiffness, based on classical composite material theory, is 7.9 MN/m. The knockdown is a result of both the hinge geometry and manufacturing imperfections. Specimen 2 has a theoretical stiffness of 2.5 MN/m; its actual stiffness was not measured. The theoretical stiffness increases for specimen 3 to 71 MN/m because this test article is fiber dominated. The measured stiffness of specimen 3 was 26 MN/m, as shown in Fig. 2a. Again, this reduction in stiffness is attributed to the hinge geometry and manufacturing processes.

Despite the knockdown, the integral folding hinge performs comparably to existing mechanical hinges. If part of the specimen 3 composite hinge is replaced with a typical mechanical hinge of length of 0.2 m and stiffness of 175 MN/m, a truss member with a net stiffness of 67 MN/m would result. This result compares favorably with the stiffness of specimen 3, which was measured to be 26 MN/m.

Axial testing of specimen 3 also indicated that the composite hinge exhibits load-cycle hysteretic properties comparable to existing precision mechanical hinge designs. Figure 2b shows that, under 44 N of load, the composite hinge exhibits approximately 1 nm of hysteresis. Comparatively, the precision hinges discussed in Ref. 11 exhibit hysteresis of approximately 1 μm under 440 N of load. Details of the structure and the testing performed can be found in Refs. 11 and 12.

In summary, the integral folding hinge appears to provide levels of stiffness and hysteresis comparable to those reported for mechanical

Table 1 Material properties for composite constituents[10]

Material property	PEEK^{TM}	IM7 carbon fibers	AS4 carbon fibers
Density, g/cm^3	1.3	1.78	1.79
Modulus of elasticity, GPa	3.5	276	228
Ultimate tensile strength, GPa	0.1	5.2	4.1

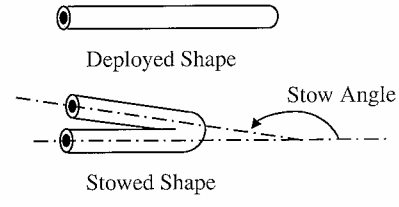

Fig. 1 Integral folding hinge in stowed and deployed position.

Table 2 Specimen geometry

Specimen	Configuration	Fiber type	Layup, deg	Length, m	Inner diameter, mm	Wall thickness, mm	Stow angle, deg
1	Laminate	IM7	±45	0.77	88.6	1.2	162
2	Braid	AS4	±45	0.66	70.3	0.41	150
3	Laminate	IM7	±5	0.90	79.99	1.65	164

hinges. It remains to be seen whether this comes at the cost of microscopic yielding in the hinge during stowage.

Experimental Apparatus and Protocols

Experimental Procedure

To assess the deployment repeatability of the integral folding hinge, several experiments were conducted on the specimens. Each test consisted of stowing the hinge for a given length of time, deploying the hinge, and measuring the position of the hinge as a function of time after deployment. Testing was conducted within a thermally stabilized chamber. This chamber, when closed out for a 24-h period, passively stabilizes the temperature of the test specimen to within tenths of a degree over a several day period and to 0.01°C for shorter, hour-long experiments.[13] In addition, the test chamber also provides passive vibration isolation that reduces the background vibration to less than 5 μg rms up to 1000 Hz (Ref. 13).

Table 3 lists the experimental variables for the study, along with how they were determined and the estimated error in each. The principal dependent experimental variables are the axial and lateral positions of the hinge tip from deployment to deployment, measured with respect to a fixed datum. These experimental variables are studied as a function of the independent variables listed in Table 3. The material properties, layup, stowage angle, ambient temperature, and specimen temperature are controlled independent variables. The number of stows, stow time, and postdeployment time are all varied.

Figure 3 shows the experimental configuration. The hinge temperature was monitored using three thermal sensors placed at various positions along the hinge, as shown in Fig. 3. The position of the hinge at the tip was measured using a videometry system. The measurement was made by recording an image of a special target placed on the test specimen. The shift in the image of the target from one image to another was calculated by a form of image correlation, which results in a relative measurement of the target motion. The principal advantage of the videometry system is that it holds its reference between images, which allows the position to be measured from one deployment to the next with respect to the fixed frame of the camera. The system and the image analysis algorithm is a derivative of the one described originally in Ref. 14 but improved to remove bias and to increase speed. This videometry system, in the highly isolated vibration environment of the testing chamber, has a total error of ±20 nm, calibrated against an interferometer with a 2.54-nm resolution. This calibration is detailed in Ref. 15.

Note that a light source was necessary to illuminate the videometry target. This fact became important because it induced a significant temperature change to the test specimen. When position was measured at shorter sample intervals (on the order of a few seconds), the light source elevated the hinge tip temperature, where the target was located, by several degrees. The error induced by the temperature change in the test specimen is discussed below.

Testing procedures had several steps. First, the test chamber was stabilized for approximately 12 h following a period of exposure to the ambient laboratory environment. The first measurement was the position of the hinge tip before the initial stowage. This initial measurement established the datum for subsequent measurements of the position of the tip. The chamber was then opened so that the hinge could be manually stowed. Time inside the chamber was minimized to control the disturbance of the thermal environment. The hinge was kept stowed for a specified period. Tests varied the stowage time from short (6-min), to medium (60-min), and long (600+-min) periods of time. The short tests were repeated multiple times. Data were collected beginning immediately following deployment. Continued measurements were made for approximately 10 times the stowage time to capture the creep behavior of the composite hinge. For the longer stow times, this period was limited by other considerations to a shorter multiple of the stowage time that varied from test to test, as listed in Table 4.

Table 3 Experiment variables

Variable	Type	Determination	Estimated error
Tip position	Dependent variable	Measured	±20 nm
Material properties	Controlled	Analysis	Unknown
Layup angle	Controlled	Measured	Unknown
Stow angle	Controlled	Measured	±0.1 deg
Ambient temperature	Controlled	Measured	±0.1 deg
Specimen temperature	Controlled	Measured	±0.01 deg
Number of stows	Varied	Counted	0
Stow time	Varied	Measured	±2 s
Postdeploy time	Varied	Measured	±2 s

Removal of Thermal Bias

As already mentioned, systematic error in the form of a thermal bias is always part of the position measurement. A linear least-squares regression was used to find a correlation between tip motion

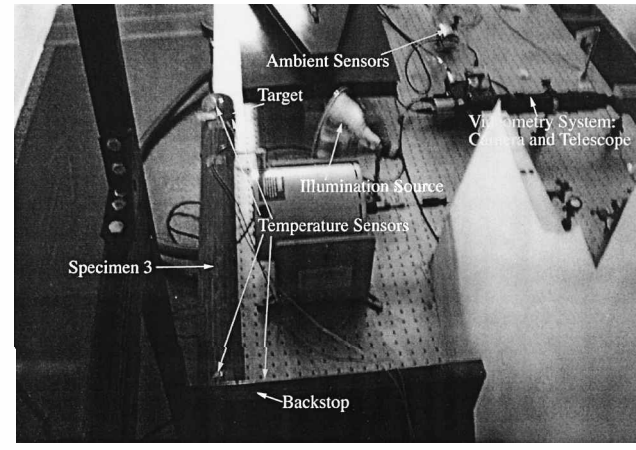

Fig. 3 Experiment configuration.

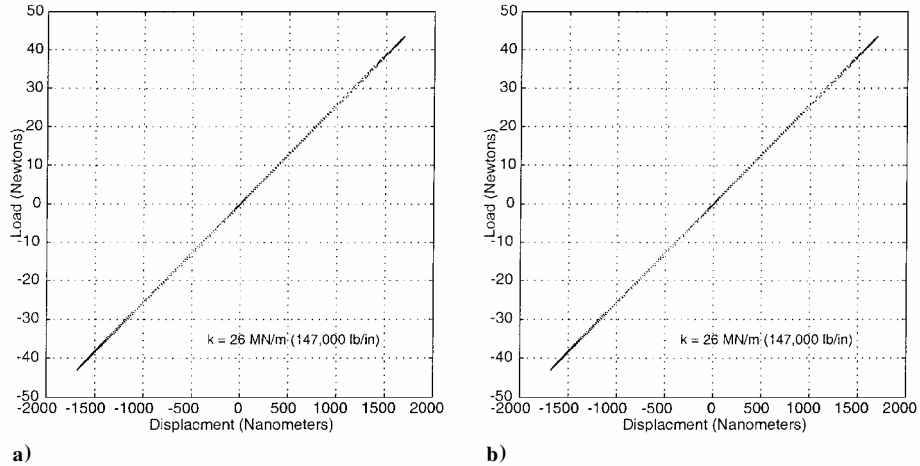

Fig. 2 Integral folding hinge under 44 N of load: a) load and b) hysteresis profile.

Table 4 Summary of test results for all integral hinge specimens

Stow length, min	No. of stows	Creep recovery, μm		Steady-state repeatability, μm	
		Axial	Lateral	Axial	Lateral
		Test article 1			
6	6	0.2–0.6	0.1–0.6	0.5–2.1	0.4–2.2
60	1	1.5	1.5	1	1
600	1	1	1	1	1
		Test article 2			
6	6	1.5–3.8	2.5–12.7	0.1–0.4	0.1–0.9
60	1	4	15	1	5
960	1	10	20	1	1
		Test article 3			
6	4	0.2–0.4	2.6–6.3	0.0–0.1	1.0–9.0
60	1	1	7	2.3	5
780	1	2	13	1.4	3

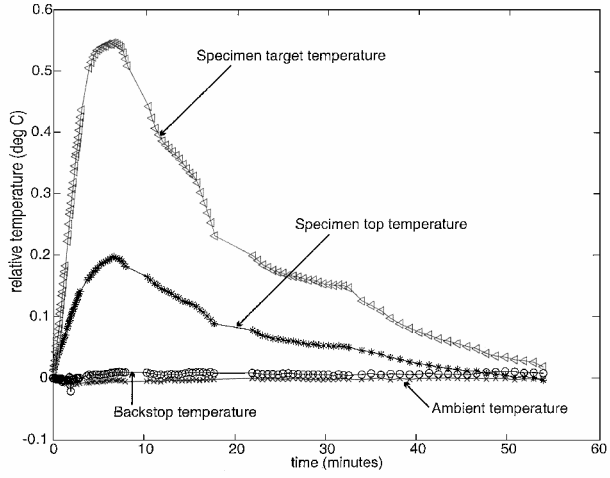

Fig. 4 Specimen 3 short stow 5 temperature profile.

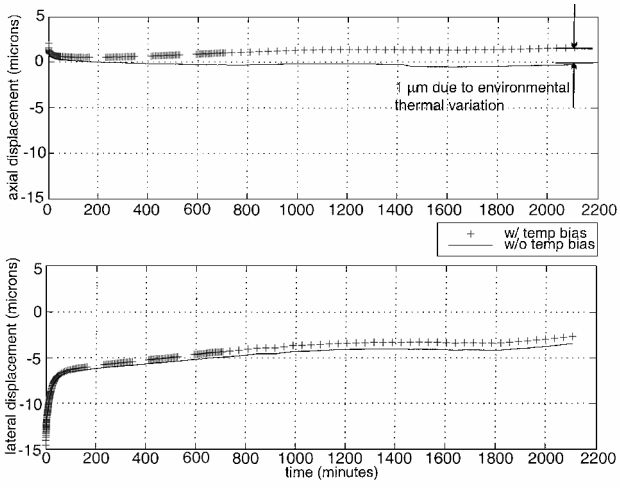

Fig. 5 Specimen 3 long stow postdeployment displacement, with and without thermal bias.

and temperature based on the following equation:

$$y = m\Delta T + b \tag{1}$$

The thermal correlation coefficient was determined from the ambient response of the tip for a period with no mechanical loading, that is, no stow–deploy cycle. This coefficient was then used to remove the thermal bias from the postdeployment results using the ambient temperature profile during each stow and deploy cycle. The ambient temperature was used for removal of the bias rather than the specimen temperature because of its quasi-static nature, whereas the specimen temperature was subject to rapid thermal variation as the videometry illumination source was cycled on and off. Figure 4 shows a typical temperature profile for a short stow cycle. Figure 5 compares the tip motion of specimen 3 after a long stow cycle with and without the thermal bias removed.

The uncertainty in removing the thermal bias was calculated using a linear regression analysis detailed in Ref. 16. This uncertainty took into account the resolution of the thermal sensors used to track temperature during experimentation, the multiple temperature samples that were averaged to determine the temperature corresponding to each tip position measurement, and the error in the curve fit to Eq. (1). The resulting 95% confidence interval for the measurements was ± 0.06 μm axially and ± 0.28 μm laterally.

Results

Representative Data

Figure 6 shows the axial and lateral hinge position after a single short (6 min) stow for specimen 3. Figure 6, which plots displacement in microns vs time in minutes, is representative of all of the data. Data were sampled at different rates, with the fastest just after deployment, when the motion rate was greatest. Slower rates later in the test were used to both minimize data storage requirements and to limit the thermal effects of the measurement system's illumination source.

There are two primary measurements tabulated for each specimen. These are the dimensional repeatability and the creep recovery. The dimensional repeatability of the hinge is defined as the absolute value of the change in the tip position from one stow to the next. As indicated in Fig. 6, the repeatability was measured as the asymptotic value that the tip position approaches some finite time after deployment. In this example, approximately an hour after deployment, the axial repeatability was measured to be 0.34 μm and the lateral was 2.39 μm. The creep recovery, also indicated in Fig. 6, was taken to be the motion from the first postdeployment sample to the sample that defined the dimensional repeatability. In this example, the creep recovery is 0.45 μm axially and 1.57 μm laterally.

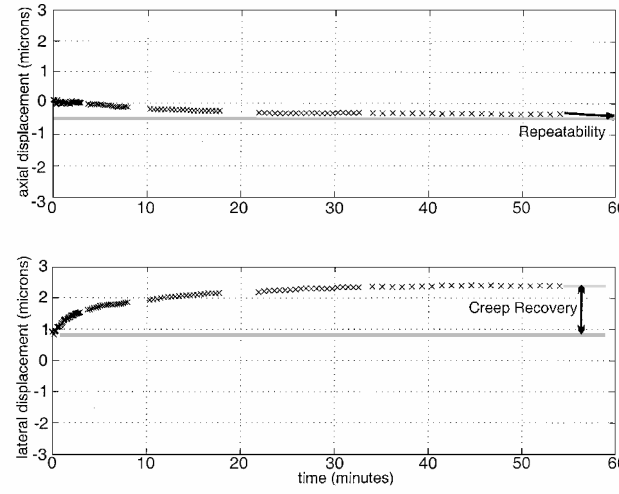

Fig. 6 Specimen 3 short stow 5 displacement results.

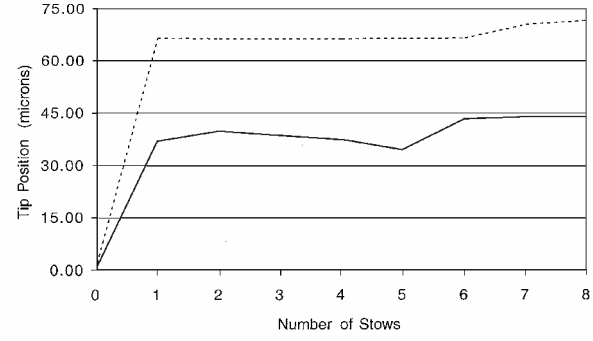

Fig. 7 Position as a function of cumulative stows for specimen 3: 2.3-μm axial and 9-μm lateral repeatability.

Effect of Number of Stows

Figure 7 plots the final tip position as function of stow number for specimen 3. Note that stow 0 indicates the position of the pristine test specimen before any stow–deployment cycles. Stows 1–6 are short (6-min) stows. Stow 7 is the medium (60-min) stow, and stow 8 is the long (780-min) stow. These data show that the specimen incurs a large amount of permanent deformation during the first stowage. After this initial deformation, the hinge converges to a new postdeployment shape. Repeated stow and deployment cycles thereafter do not cause more significant permanent deformation.

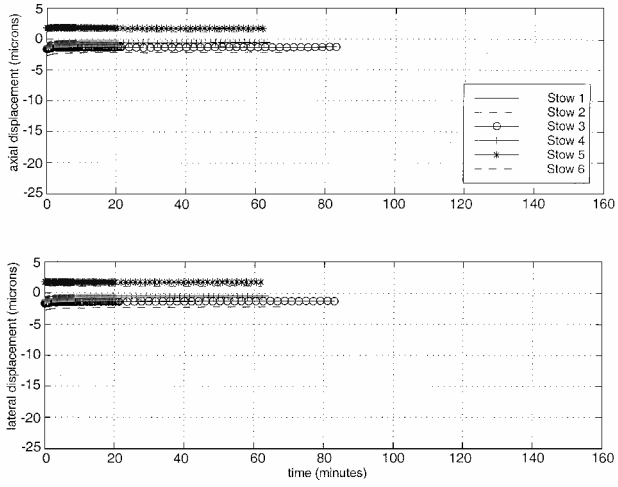

Fig. 8 Short test displacement results for specimen 1.

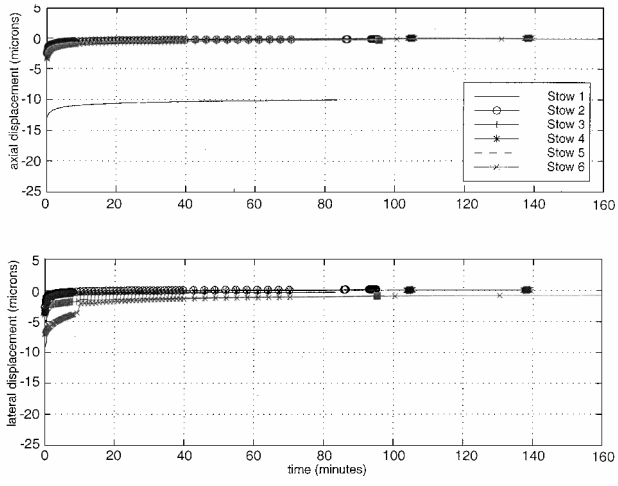

Fig. 9 Short test displacements results for specimen 2.

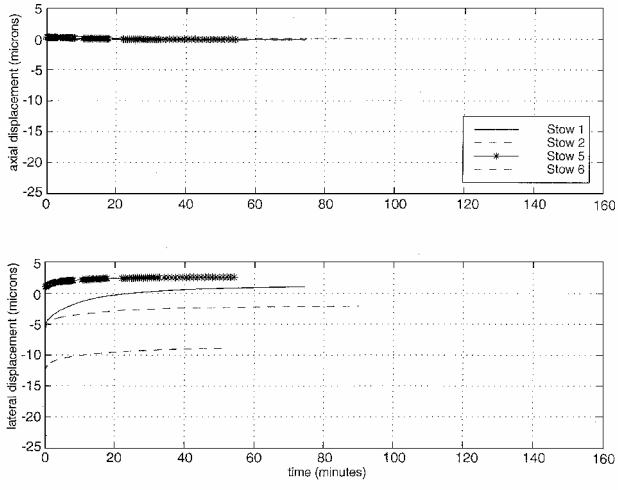

Fig. 10 Short test displacement results for specimen 3.

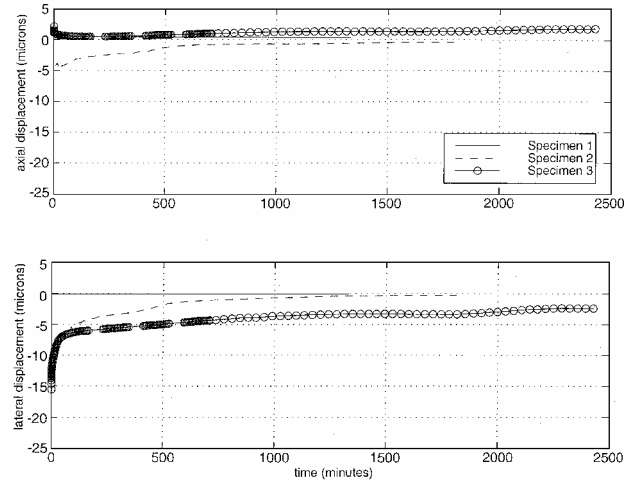

Fig. 11 Long test displacement results for all integral hinge specimens.

The permanent deformation has been identified as microscopic plasticity. Similar to the concept of microyield strength, long recognized by optical system designers and defined as the amount of stress required to produce one permanent microstrain,[9] microscopic plasticity is defined here as microscopic permanent strain that occurs below the 0.2% offset yield stress of the material. Common engineering practice is to assume that below some predetermined critical limit deformations are inconsequential, and structures are subject only to perfectly elastic behavior. However, even if the loads might be significantly below the 0.2% yield stress, nanostrain to microstrain scale permanent deformations may be induced that are unacceptable for high-precision applications, as demonstrated by the measured behavior of the specimens studied here.

Comparison of All Deployment Repeatability Data

Figures 8–10 compare the post deployment tip motion vs time of all of the short stows for specimens 1–3. In Figs. 8–10, the zero position is the position before each stow. Also, the vertical scales in each plot are all identical to provide a relative comparison of the magnitude of the observed motion. The results demonstrate that all three specimens exhibit axial repeatability better than 2.5 μm and lateral repeatability better than 9 μm. In general, the axial position is more stable than the lateral position.

Figure 11 overplots the long-term test results for all three specimens. The three specimens, despite differing composite architectures, demonstrate similar axial repeatability on the micron scale. The lateral repeatability differs by less than 5 μm. At the time of the long-term test, all three specimens had accumulated between 8 and 10 stow–deploy cycles.

Table 4 summarizes the test results. The dimensional repeatability varies among the specimens from 0 to 2.5 μm axially and from 0.1 to 9 μm laterally. The creep recovery ranges between 0.5 and 10 μm axially and between 0.5 and 20 μm laterally.

These results lead to several observations. The material properties have the greatest effect on the magnitude of creep recovery. Creep recovery is smallest in the $\pm$45-deg laminated specimen (specimen 1) and greatest in the braided (specimen 2). Of the two laminated specimens, 1 and 3, the axially fiber-dominated one (specimen 3) shows a larger lateral creep recovery. Presumably, this is due to the lateral motion being dominated by the matrix, which has a higher viscoelastic compliance than the fibers.

There does not appear to be a sensitivity to stow duration or number of stows. The number of repeated stows and deployments does not effect the repeatability, once the initial stow occurred. As stow time increases, the repeatability is within 5 μm both axially and laterally. The creep recovery, however, does depend on stow time. As stow time increases, the creep recovered and the amount of time recovery took does as well. This behavior is consistent with viscoelastic theory. (An estimate of the equivalent viscoelastic time constant is presented in the next section of this paper.)

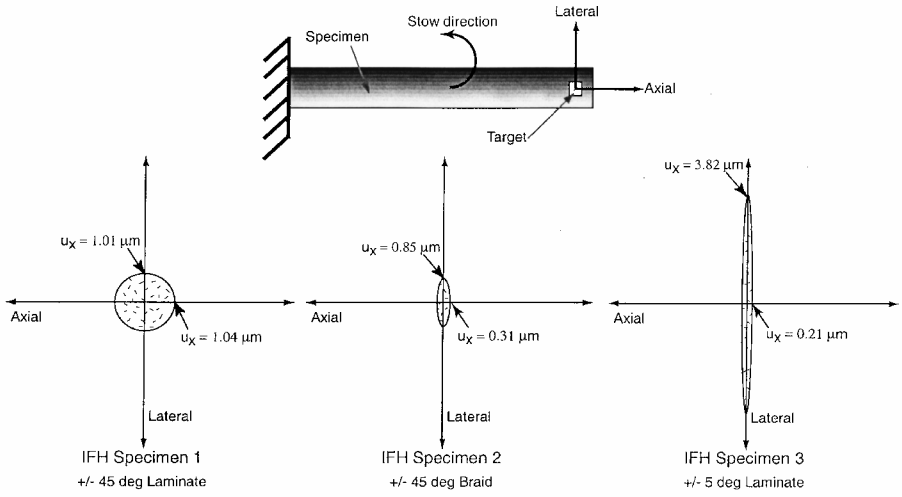

Fig. 12 Precision intervals for all three specimens.

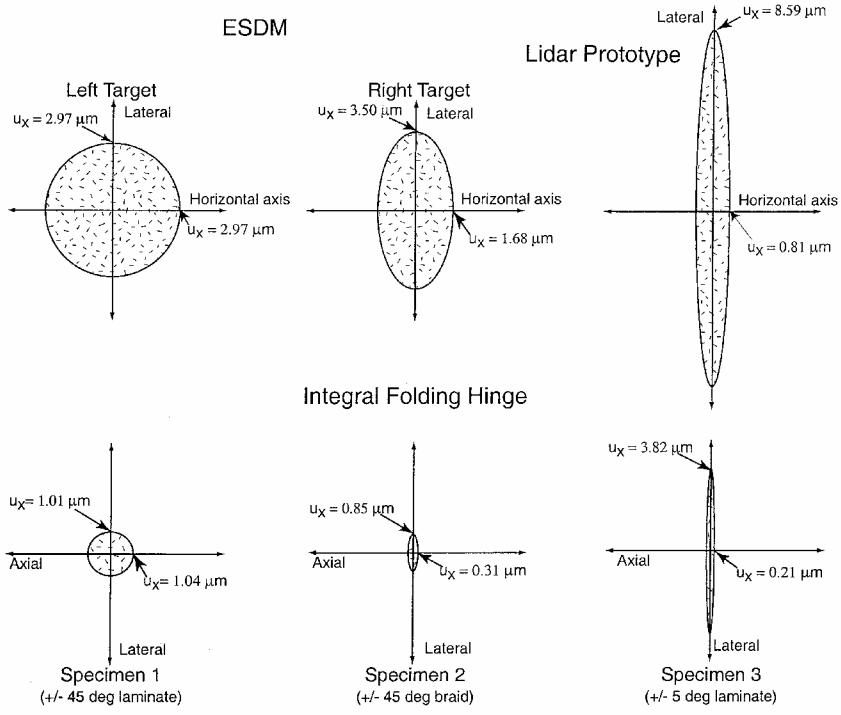

Fig. 13 Comparison of precision intervals for three precision deployment systems.

Only a finite number of tests were conducted, so the measures of dimensional repeatability need to be corrected for the finite statistics, using the following relation:

$$u_x = t_{v,P}\left(S_x \Big/ N^{\frac{1}{2}}\right) \tag{2}$$

For the data presented here, the probability is fixed at 95%, and all other variables depend on the specimen under consideration.

Figure 12 graphically displays the precision intervals for all three specimens tested. All three specimens demonstrate similar width intervals in the axial direction, but differ in the lateral direction. The increased size of the precision interval in the lateral direction for specimen 3 is, once again, attributed to the fact that this is the off-axis direction of this fiber-dominated specimen. These results indicate that repeatability of the composite folding hinge is consistent and within an acceptable range for precision deployment applications.

It is useful to compare these results with the deployment repeatability of a mechanically deployed structure of similar size and stiffness. In the experiments presented in Refs. 11, 12, and 15, the deployment repeatability of two mechanically deployed reflector petals was measured, and the resulting P95% precision intervals calculated in Ref. 15. Figure 13 compares the precision intervals of those two structures and the integral folding hinge. The two systems used for the comparison are the Engineering Science Development Module (ESDM)[14] and the Lidar Prototype.[14] Both systems are 1-m-class single petals of a multipetal reflector that were cantilevered for experimentation. The deployment repeatability was measured with the same videometry system discussed in this paper. The integral folding hinge demonstrated deployment repeatability comparable to the known literature references of the repeatability of these precision deployables.

Analysis of the Viscoelastic Time Constants

It is important to understand whether the creep recover time profile is consistent with a linear viscoelastic model. This hypothesis can be tested by fitting the following general exponential response to the data:

$$\hat{y}(b, \{a\}, \{\tau\}) = b + \sum_{m=1}^{M} a_m \exp\left(-\frac{t}{\tau_m}\right) \tag{3}$$

Note that the presence of the nonzero constant offset term b does not allow a simple linear fit to be used in a logarithm time domain. For this reason, the parameters are estimated by minimizing the

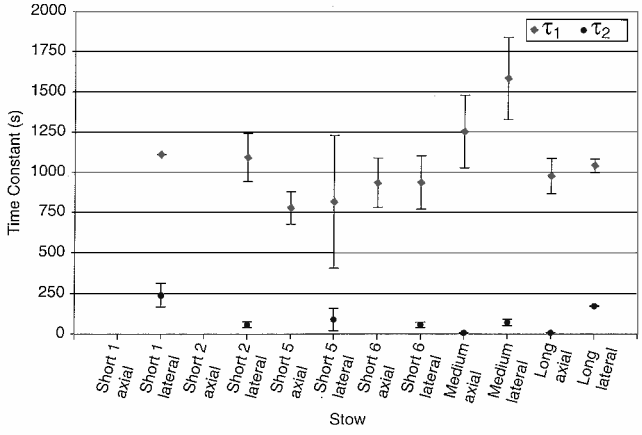

Fig. 14 Specimen 3 viscoelastic time constants.

chi-squared error:

$$\chi^2 = \sum_{i=1}^{N} \frac{[y(t_i) - \hat{y}(t_i)]^2}{\sigma_i^2} \tag{4}$$

in which the data standard deviations are taken to be the confidence intervals determined for the respective measurements. A Levenberg–Marquardt minimization algorithm was used to minimize this function (see Ref. 17). The initial search values are randomized to determine convergence to a global minimum. Statistical sensitivity is used to develop confidence intervals for the estimated model parameters.

The results indicate that the viscoelastic behavior is not well modeled by a single exponential, but by two. One of the time constants is typically on the order of hundreds of seconds and one is on the order of tens of seconds. In Fig. 14, the time constants calculated for specimen 3 are plotted along with the confidence intervals of the estimates. It appears from the data that the time constants are, within the confidence intervals of the estimates, approximately independent of stow duration. This inclusiveness indicates that the creep recovery is governed by linear, time-invariant mechanics, the nature of which awaits further theoretical investigation.

Conclusions

This paper experimentally assesses the deployment repeatability of a novel folded composite hinge. The hinge is an integral feature of a composite tube intended for use as a structural truss member in a high-precision application. The flexure design of the hinge allows the tube to be elastically folded for stowage in spite of the large wall thickness, which gives the tube high stiffness. This paper also experimentally assesses whether the large but elastic folding stresses impart permanent deformations to the tube after it is deployed. The data show that any such permanent strain, identified as microscopic plastic behavior, induces no more 2.5 μm axially and 9 μm laterally of tip deformation, depending on the composite layup with maximum precision intervals of 1.04 μm axially and 3.82 μm laterally. This deployment repeatability is comparable to prior measurements of mechanical deployables. Moreover, stow duration and number of stows have no measurable effect, once the initial stow–deploy cycle has been completed. There is always a significant viscoelastic creep recovery following deployment that increases with stowage time. However, this viscoelastic creep is recovered. An analysis of the creep shows that it is well predicted by a linear exponential model with two time constants that are independent of stow duration. These results partially validate the use of this type of hinge for consideration in precision deployables, to the level of resolution of these experiments.

Acknowledgments

This research was sponsored by Foster Miller, Inc., under U.S. Department of Defense Small Business Innovation Research (SBIR), Contract F29601-99-C-0010. R. Scott Erwin is the SBIR Technical Monitor at the U.S. Air Force Research Laboratory Space Vehicles Directorate.

References

[1]Bely, P.-Y., "The NGST 'Yardstick' Mission," *Proceedings of the 34th Liege International Astrophysics Colloquium*, Liege, Belgium, 1998, pp. 159–166.

[2]Lake, M. S., Peterson, L. D., Hachkowski, M. R., Hinkle, J. D., and Hardaway, L. R., "Research on the Problem of High-Precision Deployment for Large-Aperture Space-Based Science Instruments," *Proceedings of the 1st Conference on Global Virtual Presence and 1st Conference on Orbital Transfer Vehicles*, STAIF, Albuquerque, NM, 1998, pp. 188–198.

[3]Mikulas, M. M., Jr., Bush, H. J., and Card, M. F., "Structural Stiffness, Strength and Dynamic Characteristics of Large Tetrahedral Space Truss Structures," NASA TM-X-74001, March 1977.

[4]Iqbal, K., Pellegrino, S., and Daton-Lovett, A., "Bi-Stable Composite Slit Tubes," *IUTAM–IASS Symposium on Deployable Structures: Theory and Applications*, edited by S. Pellegrino and S. D. Guest, Kluwer Academic, 2000, pp. 153–162.

[5]Rimrott, F. P. J., and Draisey, S., "Critical Bending Moment of Double-Slit Tubing," *Journal of Spacecraft and Rockets*, Vol. 21, No. 3, 1984, pp. 316–318.

[6]Rimrott, F. P. J., "Two Secondary Effects in Bending of Slit Thin-Walled Tubes," *Journal of Applied Mechanics*, Vol. 33, No. 1, 1966, pp. 75–78.

[7]Seffen, K. A., and Pellegrino, S., "Deployment Dynamics of Tape Springs," *Proceedings of the Royal Society of London, Series A: Mathematical and Physical Sciences*, Vol. 455, 1999, pp. 1003–1048.

[8]Seffen, K. A., You, Z., and Pellegrino, S., "Folding and Deployment of Curved Springs," Dept. of Engineering, Univ. of Cambridge, TR CUED/D-STRUCT/TR 171, Cambridge, England, U.K., Dec. 1997.

[9]Marschall, C. W., and Maringer, R. E., *Dimensional Stability: An Introduction*, 1st ed., Pergamon, New York, 1977.

[10]Gautheir, M. M. (ed.), *Engineered Materials Handbook*, American Society for Materials International, Materials Park, OH, 1995.

[11]Warren, P. A., Peterson, L. D., and Hinkle, J. D., "Submicron Mechanical Stability of a Prototype Deployable Space Telescope Support Structure," *Journal of Spacecraft and Rockets*, Vol. 36, No. 5, 1999, pp. 765–771.

[12]Warren, P. A., and Peterson, L. D., "Sub-Micron Non-Linear Shape Mechanics of Precision Deployable Structures," Ph.D. Dissertation, Dept. of Aerospace Engineering Sciences, Univ. of Colorado, Rept. CU-CAS-96-18, Boulder, CO, July 1996.

[13]Hardaway, L. M. R., and Peterson, L. D., "Stability and Mechanics of Precision Deployable Structures Under Nanometer Deformation," Ph.D. Dissertation, Dept. of Aerospace Engineering Sciences, Univ. of Colorado, Rept. CU-CAS-00-12, Boulder, CO, May 2000.

[14]Hinkle, J., and Peterson, L. D., "A Micron-Precision Metrology System for Measuring Structural Geometric Repeatability," M.S. Thesis, Dept. of Aerospace Engineering Sciences, Univ. of Colorado, Rept. CU-CAS-95-16, Boulder, CO, Aug. 1995.

[15]Heald, J. C., and Peterson, L. D., "Deployment Repeatability of a Space Telescope Reflector Petal," *Journal of Spacecraft and Rockets*, Vol. 39, No. 5, 2002, pp. 771–779; also AIAA Paper 2001-1302, April 2001.

[16]Figliola, R. S., and Beasley, D. E., *Theory and Design for Mechanical Measurements*, 2nd ed., Wiley, New York, 1995.

[17]Press, W. H., Flannery, B. P., Teukolsky, S. A., and Vetterling, W. T., *Numerical Recipes: The Art of Scientific Computing*, 1st ed., Cambridge Univ. Press, New York, 1986.

J. Lassiter
Guest Editor